

Flapping dynamics of a flexible filament

H. Ait Abderrahmane and M. P. Paidoussis

Department of Mechanical Engineering, McGill University, Montreal, Quebec H3A2K6, Canada

M. Fayed and H. D. Ng

Department of Mechanical and Industrial Engineering, Concordia University, Montreal, Quebec H3G 1M8, Canada

(Received 11 August 2011; revised manuscript received 16 November 2011; published 14 December 2011)

This paper investigates the dynamics of the flapping regime of a filament placed in a two-dimensional soap-film flow for different filament lengths and flow speeds. It was found that the onset of flapping is quasiperiodic, with the main flapping amplitude and frequency modulated by low-amplitude, low-frequency oscillation. At higher flow velocities, the oscillation becomes chaotic. The transition to chaos occurs via the quasiperiodic route to chaos. A new bistability phenomenon was discovered in which the system alternates between the stretched-straight and oscillatory states, which is here referred to as “switching oscillation.” Unlike some previously reported forms of bistability, in this case the system alternates between the two states continuously, without any external perturbation.

DOI: [10.1103/PhysRevE.84.066604](https://doi.org/10.1103/PhysRevE.84.066604)

PACS number(s): 46.40.–f

I. INTRODUCTION

Oscillation or “flapping” of platelike structures in axial flow has been the subject of a great deal of study by the science and engineering research communities, because it arises in many situations in nature and in engineering applications. Examples are the oscillation of web in paper making, fluttering of flags, oscillation of plant leaves, vibration of the soft plate in snoring, vibration in parallel-plate-type heat exchangers, flutter in “flutter mills” used for power generation, and many others. Perhaps the first study of this subject was made by Rayleigh [1], who pointed out the similarities between the flapping of a flag and jet undulations. A multitude of studies then followed; see, for instance, the monograph by Dowell [2], the book by Paidoussis [3], and the review by Shelley and Zhang [4].

Some theoretical studies that should be mentioned are those by Kornecki *et al.* [5] and Huang [6] using Theodorsen’s theory [7], Yamaguchi *et al.* [8] using a linearly varying vortex theory, Watanabe *et al.* [9] and Balint and Lucey [10] using respectively compressible and incompressible two-dimensional (2D) Navier-Stokes solvers, Guo and Paidoussis [11] and Eloy *et al.* [12,13] using potential flow theory, Argentina and Mahadevan [14] using a simplified Theodorsen model, Tang and Paidoussis [15] using vortex panel method, Alben and Shelley [16] using a nonlinear vortex sheet, and Michelin *et al.* [17] using discrete-point vortices with unsteady strengths.

Several other numerical approaches had been developed for the flapping flag in viscous fluid flow. For instance, Zhu and Peskin [18] used the immersed boundary method, and Connell and Yue [19] developed a fluid-structure direct-simulation capability that couples a direct numerical simulation of the Navier-Stokes equations to a solver for thin-membrane dynamics.

There exists a wealth of experimental studies in the literature as well, starting with Taneda [20], who had investigated many types of flag, some made of loosely woven material. Other notable studies are the wind tunnel experiments

conducted by Huang [6], Yamaguchi *et al.* [21], Wanatabe *et al.* [22], Tang *et al.* [23], and Eloy *et al.* [12] and the water tunnel experiments by Shelley *et al.* [24], as well as the soap-film tunnel experiments by Zhang *et al.* [25], which are of particular interest here.

Most of these numerical and experimental studies reported three different states for the structure: the stretched-straight state where the structure is aligned with the flow and does not flap, and the regular flapping and irregular flapping states. They reported also a bistability phenomenon and hysteresis of the stretched-straight and flapping states. However, most of the past and recent studies mainly focused on the instability threshold; few showed much interest in the dynamics of the flapping and its underlying mechanisms, for example, Connell and Yue [19], Alben and Shelley [16], and Michelin *et al.* [17]. These authors attempted a characterization of the flapping in terms of spectral analysis and dynamical systems theory to describe the transition from a regular into an irregular state and capture the inherent bistability of flapping and stationary states. These theoretical studies have shown that it is possible to characterize the dynamics of the flapping through the evolution of frequency power spectra and of system attractors in phase space.

This paper is an experimental study on the nonlinear dynamics of a flapping flag by experiments using filaments in soap-film flow. The dynamics is analyzed using a nonlinear time-series method. This paper reports for the first time a robust phenomenon of “switching oscillations,” where the system switches from one type of oscillatory state to static equilibrium and back again, which may be viewed as a form of bistability associated with hysteresis. The switching-oscillations phenomenon manifests itself without any external action; that is, the filament dynamics continuously switches between two states: the stretched-straight and flapping states. This manifestation of bistability differs from the one previously reported in Taneda [20], Connell and Yue [19], and Shelley and Zhang [4], where an external perturbation is needed to shift the system from the stretched-straight state to the flapping one and the system remains in that

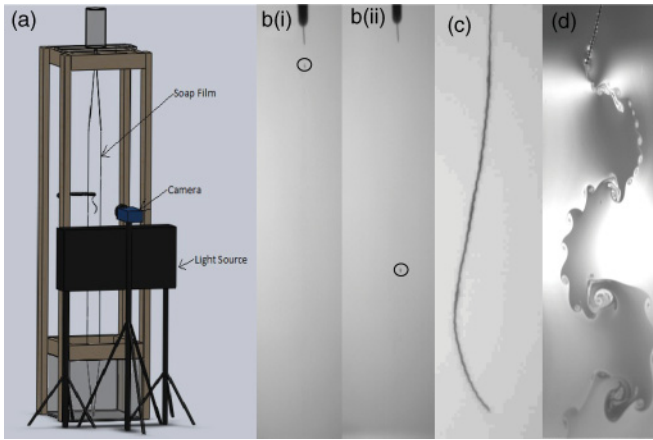


FIG. 1. (Color online) Experimental details: (a) experimental setup, (b) flow-speed measurement technique, (c) flapping filament, and (d) wake behind a flapping filament.

state permanently, without ever returning to the stretched-straight state. Like bistability, the phenomenon of switching oscillations can be considered as a benchmark problem in this field.

II. EXPERIMENTAL SETUP

The experiments were conducted in a two-dimensional flow apparatus that consists of a vertical gravity-driven flowing soap film; see Fig. 1(a). The soap film was made of a 1% solution of a commercial brand of dishwashing liquid soap (Dawn) in water, which was supplied through a nozzle from a reservoir. The planar soap film was produced by guiding the soapy water via taut nylon threads (1 mm in diameter) spreading out to the desired width (15 cm). The silk filament was maintained within the flow by fixing its leading end with a very thin needle.

The flow rate was adjusted through the gear pump, which for steady conditions resulted in a constant fluid height in the reservoir. The reservoir served to inhibit flow perturbations, and this ensured a constant pressure head at the nozzle, quasiconstant flow speed, and relatively homogeneous film thickness at the test section. The filament was located sufficiently far downstream from the nozzle (approximately at a distance of 1 m) where a balance between the main forces (inertial, elastic, gravitational, and drag forces) at work in such a gravity-driven soap film tunnel should have been reached and the flow should have reached asymptotically its terminal velocity and constant thickness, as predicted by the well-known experiments of Georgiev and Vorobieff [26] and Rutgers *et al.* [27]. The flow velocity was measured by tracking a small droplet of dye transported by the flow; see Figs. 1[b(i)] and 1[b(ii)]. This value of the velocity has been verified by tracking the center of vortices shed by the flapping filament and the very small air bubbles present in the soap film. Typical flow velocities in our experiments ranged between 4.3 and 8.5 m/s. The silk filament has the following properties: mass per unit length $\rho = 0.01$ g/m and diameter $d = 0.04$ mm. Its flexural rigidity was estimated using the following relation: $D = \rho g L^3 / 8H$, where ρ , g , H , and L are the mass per unit length, acceleration due to gravity, deflection of the cantilevered fiber under its own weight, and length of

the fiber, respectively; see Dadeppo and Schmidt [28]. Soap film tunnels provide an opportunity to realize two-dimensional flows [29,30]. Nevertheless, measuring the pertinent physical parameters, such as surface viscosity and film thickness, is not trivial; see Martin and Wu [31] and Wu *et al.* [32]. Martin and Wu remarked that a more systematic method to measure film viscosity remains to be developed. In the present paper, we used the method based on the empirical relation suggested by Roshko [33], which relates the Strouhal and Reynolds numbers in von Karman vortex shedding behind a circular cylinder. Gharib and Derango [30] showed that 2D von Karman vortices behave the same as the three dimensional (3D) one. In the range of flow velocities considered in our experiments and the dimensions of our experimental setup, the kinematic viscosity of the film was found to vary from 96 to 270 times the viscosity of the water. The Reynolds number (Re) in our experiments is defined as VL/ν , where V , L , and ν stand for flow velocity, length of the filament, and kinematic viscosity of the soap film, respectively. The second physical parameter of the soap film is its thickness and its fluctuations. As remarked by Wu *et al.* [32], the film thickness measurement is also not trivial; in this paper we estimated the film thickness based on the conservation of mass. In fact, the thickness of the film can be determined by the flow rate measured at the nozzle, the measured velocity at the test section, and the width of the channel. The estimated film thickness for our experiments varied between 0.8 to 1.7 μm . As the flow speed is lowered, the film becomes thinner. In these conditions, we did not observe striations or interference in the soap film illuminated by a low-pressure sodium light. In general, the film thickness increases with increasing flow speed and further it becomes susceptible to fluctuations. Under these conditions, the fluctuations of the soap-film thickness manifest first as striations along the flow, which become transversal to the flow at higher flow speeds. The maximum flow speed in our experiments was 8.5 m/s and, if we assume for Marangoni elasticity the value given in Couder *et al.* [29], we estimated the celerity of the symmetrical elastic wave for our experimental conditions (film thicknesses varying between 0.8 and 1.7 μm) to vary between 9.7 and 14.4 m/s. The maximum flow speed is inferior to the minimum value for symmetric elastic waves; hence, the flow is subcritical. Moreover, the subcritical character of the flow can be accessed based on patterns formed by striations or the interferences. In conditions of high flow velocity, the flow patterns consist of striations that differ from the diamond patterns that characterize supercritical flow. In fact, such diamond patterns were observed in the upstream wedge, while around the test section such patterns were not observed. This means that far upstream flow was supercritical and had undergone transition through *Marangoni shocks* to subcritical flow far downstream in the test section. It was argued that such thickness fluctuations behave as a passive scalar field like diffusion of a dye in flow [34].

The motion of the flapping filament was recorded using a high-speed camera at a rate of 800 images per second. Typical images are shown in Figs. 1(c) and 1(d). The images were processed, and the time history of the displacement amplitude of a point on the filament, located at $\frac{1}{3}$, $\frac{2}{3}$, and $\frac{3}{4}$ of its length when it was stretched straight and aligned with the flow, was extracted. The flapping dynamics of these three points were found to be identical; in the following we present only the one

deduced from the displacements of the points located $\frac{3}{4}$ of the filament length.

Three main dynamical states were observed. The first one is the stretched-straight state, which was observed at small flow velocities. In this state, the filament was aligned with the flow and remained stationary until the critical flow velocity was reached. Above the critical flow velocity, the filament spontaneously started flapping, and this is referred to as the second dynamical state. With further increase of the flow speed, the flapping dynamics became more and more complex, and this is referred to as the chaotic flapping state.

The experimental procedure is as follows. First, the flow velocity was set to a small value, at which the filament remained stretched straight. The flow velocity was then increased gradually until the critical value, U_c . The flow velocity was then further increased up to the maximum attainable by the experimental setup (8.5 m/s). Afterward, the flow velocity was decreased, with the same steps as before, until the filament returned to its initial stable state. In the case of long filaments, the critical speed for cessation was much lower than for onset of flapping, which indicated a hysteresis phenomenon.

The dynamics of the flapping regime was further investigated using the nonlinear time-series analysis technique of the amplitudes of the aforementioned point on the flexible filament. This technique was proposed by Packard *et al.* [35]; it consists of the reconstruction of a multidimensional phase portrait, which helps to reveal the dynamical behavior of the system, from measurements of a single variable. The procedure relies on the reconstruction of the whole system trajectory in an *embedding space*, using the *delay-time* method of Takens and Mañé [35,36]. To ensure equivalence between the topological properties of the actual and reconstructed attractors as well as to provide further characterization of the attractors reconstructed from the time series, techniques such as the well-known Grassberger-Procaccia algorithm [37] and the interactive method by Albano *et al.* [38], which take into consideration the inherent noise within the data, can be used to determine the dimension of the attractors, that is, a measure of complexity of the attractor. Particularly, the correlation dimension can be used to differentiate between deterministic and stochastic chaos.

III. RESULTS AND DISCUSSION

The flapping dynamics is discussed by first looking at the evolution of power spectra and the results from the nonlinear time-series analysis. Using the embedding or delay-time method, the attractors that describe the nonlinear dynamics of the flapping in phase space were reconstructed from the transverse displacement time series of the chosen point on the filament. To reduce the influence of intrinsic noise in the time series, we have first performed empirical mode decomposition as proposed in Huang *et al.* [39]. The empirical mode decomposition EMD method was developed to analyze nonlinear and nonstationary time series. The idea was to separate a given signal into its constitutive parts with different frequencies. Here, we follow the algorithm proposed by Huang *et al.* [39] to perform EMD on the experimental results. This consists of the following steps: First, the local extrema of the

time trace are identified. Second, the local maxima and minima are interpolated to construct upper and lower envelopes. Third, the local detail is obtained by subtracting the average of the envelopes from the original time trace. The resulting time trace is an intrinsic mode function (IMF) if it satisfies the following conditions: (i) the time trace has a mean value equal to zero and (ii) it has only one extreme between the zero crossings. If these two conditions are satisfied, then the residual (i.e., the difference between the original time trace and the first IMF) is determined and used for the next loop. After several iterations, the residual (and therefore the resulting IMF) become negligible. To this end, the original time series can be expressed as the sum of the intrinsic mode functions and the residual. Using this method, the time traces measured in this study are decomposed into IMFs; however, it appears that the main dynamics is contained only in the first intrinsic mode. The other modes are of small amplitude and they are considered as intrinsic noise. For instance, the amplitude of the second IMF is less than 1.5% of the first one. The dominance of the first intrinsic mode can be justified through the comparison of the power spectra of the original time series and the first IMF. In other words, the one that corresponds to the first IMF is similar to the one obtained from the original time trace. The main difference is that the first one contains less noise.

A. Flapping dynamics

In general, the flapping dynamics of a filament can be controlled through two control parameters: filament length and flow velocity. The variation of these control parameters is equivalent to the variation of the three nondimensional parameters, i.e., filament-to-fluid mass ratio, Reynolds number, and bending rigidity. This work considered different filament lengths and flow speeds, which correspond to different values of these governing parameters. In all the experiments, it was found that the flapping dynamics was qualitatively the same; hence, in the following the discussion is restricted to the presentation of only the results obtained for the 2-cm-long filament.

Figure 2 is related to the flapping regime of this filament just after flapping onset. Snapshots of the flapping regime are shown in Fig. 2(a); one can easily notice that, because of gravity and flow-induced tension, approximately one-tenth of the filament length is inactive and remains almost in the stretched-straight state. The raw time series of the displacement amplitude of a point located at $\frac{3}{4}$ of the filament length is shown in the top graph of Fig. 2(b); from this, the first and second intrinsic modes have been extracted and are shown in the two lower graphs of Fig. 2(b).

A frequency analysis was first performed on the first intrinsic mode, and the resulting power spectrum is shown in Fig. 2(c). The power spectral density exhibits a flapping mode with fundamental frequency (f_1) equal to 81.2 Hz and its harmonics. The power spectral density also reveals the presence of a small-amplitude low-frequency component with a dominant frequency f_2 approximately equal to 1.6 Hz. It is worth noting that such a small-amplitude low-frequency oscillation was also captured by Alben and Shelley [16] using their numerical vortex-sheet model.

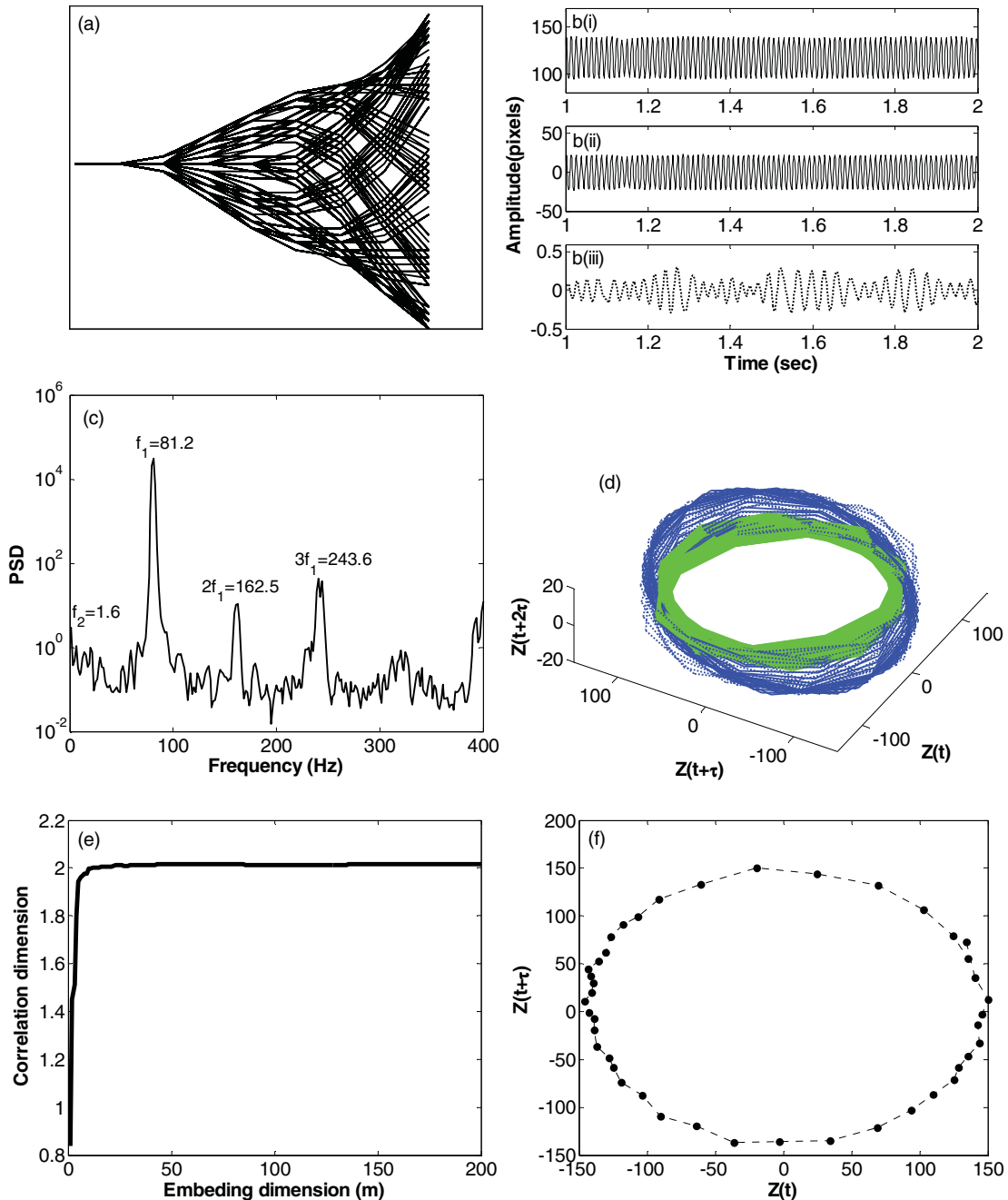


FIG. 2. (Color online) Spectra and dynamical analysis: (a) snapshots of the 2-cm-long filament for flow speed of 6.36 m/s; (b) time series of the cross-stream displacement of a point located at $\frac{3}{4}$ of filament length: (i) raw time series, (ii) first intrinsic mode, and (iii) second intrinsic mode; (c) power spectrum of the cross-stream displacement; (d) reconstructed attractor in principal basis from the time series of the cross-stream displacement; (e) correlation dimension of the reconstructed attractor; and (f) Poincaré section of the attractor in (d).

In the flapping regime, the oscillation is quasiperiodic [40]. Since the order of magnitude of the f_2 component is approximately fifty times smaller than the f_1 component, it is difficult to perceive its influence via the power spectrum, which does not provide any information about the underlying dynamics and the way these two frequency components interact. Therefore, a dynamical analysis is performed where the attractor that depicts the dynamics of the system is reconstructed from the first intrinsic mode time series in Fig. 2[b(ii)]. To ensure a diffeomorphism between the unknown actual

attractor and the reconstructed one, Takens’s criterion was used. The corresponding attractor of the flapping state is a tiny cross-sectional torus; however, for the analysis of the flapping dynamics, the attractor was projected onto the principal basis [38] [see Fig. 2(d)]. The advantage of this projection is that it allows filtering out a large amount of the remaining noise in the time series. Figure 2(d) clearly shows that the 3D projection on the principal basis is a torus, which confirms that the flapping regime is quasiperiodic. As shown in Fig. 2(e), the estimated correlation dimension of the attractor is close

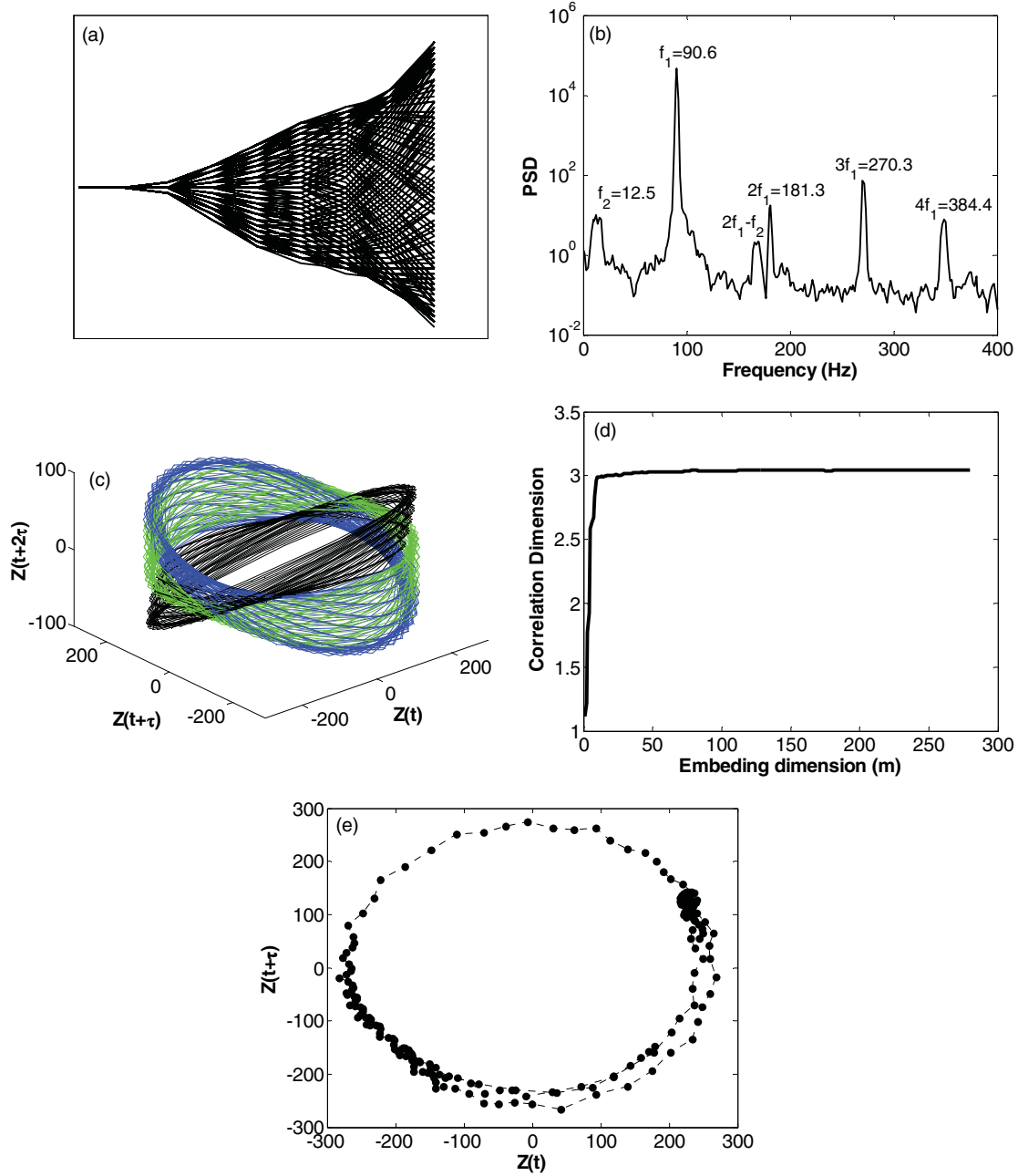


FIG. 3. (Color online) Spectra and dynamical analysis: (a) snapshots of the 2-cm-long filament for flow speed of 7.8 m/s; (b) power spectrum of the cross-stream displacement; (c) reconstructed attractor in principal basis from the time series of the cross-stream displacement; (d) correlation dimension of the reconstructed attractor; (e) Poincaré section of the attractor in (c).

to 2 ($D = 1.96$). It is worth noting that this estimated value remains constant with the embedding dimension and varies slightly (approximately 5%) when longer time series were considered.

To verify further the correspondence between the spectral and dynamical analysis results, a Poincaré section on a plane parallel to the $[Z(t), Z(t + \tau)]$ plane of Fig. 2(d) is plotted in Fig. 2(f). The Poincaré section is an ensemble of discrete points distributed on a closed curve, which further confirms the quasiperiodic nature of the flapping. The mean time durations of each of the two oscillation components, namely the main oscillation component at the onset of flapping and

its modulation, are estimated. The mean frequency of two successive crossings of the Poincaré section is approximately 82.2 Hz, which is close to the flapping frequency f_1 obtained by spectral analysis. On the other hand, the approximate frequency of one rotation of a crossing point (a complete lap) is 1.9 Hz, which can be considered fairly close to the frequency f_2 in the power spectral density (PSD). Hence, both spectra and nonlinear time-series analysis indicate that the flapping filament dynamics is modulated by oscillations of relatively small amplitude and frequency.

By increasing further the flow speed, it is observed in the power spectrum that the frequencies of the flapping (f_1) and

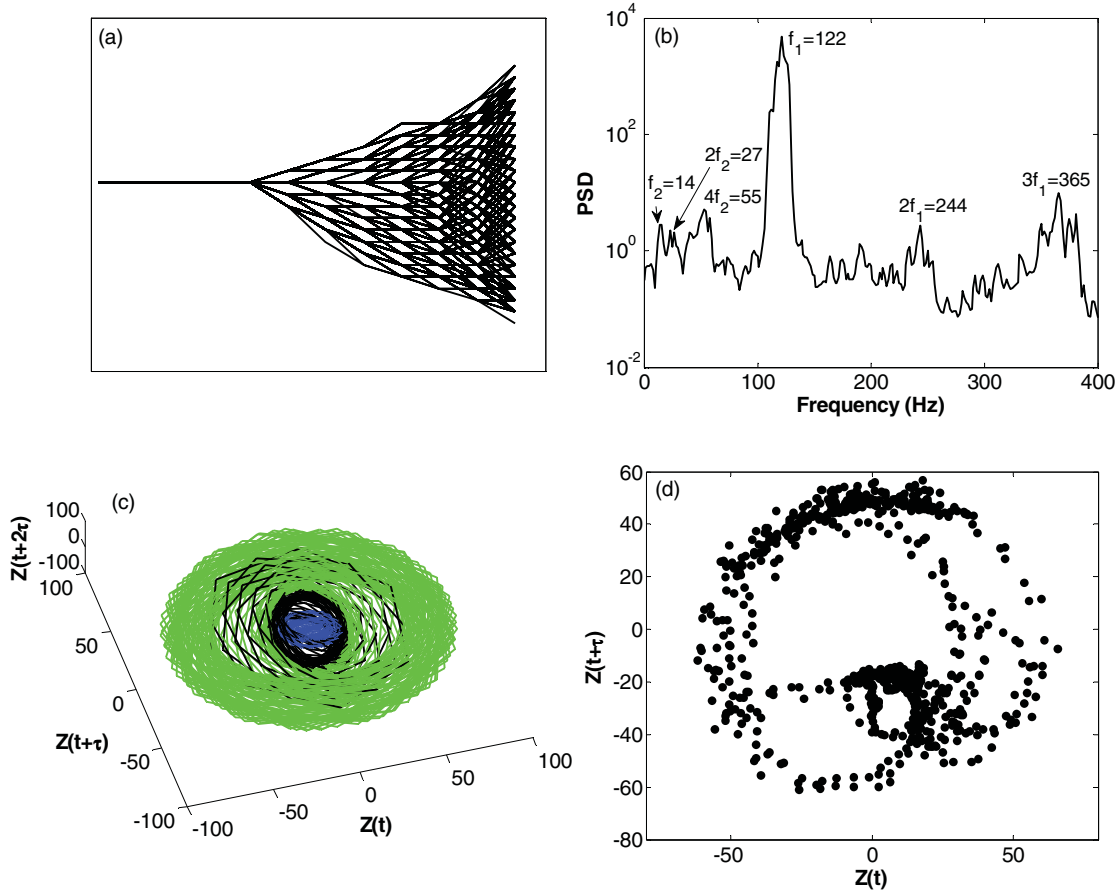


FIG. 4. (Color online) Spectra and dynamical analysis: (a) snapshots of the 2-cm-long filament for flow speed of 8.5 m/s; (b) power spectrum of the cross-stream displacement; (c) reconstructed attractor in principal basis from the time series of the cross-stream displacement; and (d) Poincaré section of the attractor in (c).

its modulation (f_2) increase; see Fig. 3(a). The regime remains quasiperiodic. Similar to the preceding case, a nonlinear time-series analysis is performed. The 3D projection of the attractor remains toruslike, but its dimension has now increased by approximately 1; the estimated correlation dimension of the attractor ($D = 2.94$) is very close to 3, which indicates that the flapping dynamics has become more complex. The Poincaré section remains formed of discrete points distributed on a closed curve, and it is noticed that a ringlike structure starts to form. This indicates that the trajectories seem to start abandoning the torus, which begins to be destroyed. By increasing further the flow speed to the maximum velocity allowed by the experimental setup ($V = 8.5$ m/s), it is observed in Fig. 4(b) that the frequency that corresponds to the flapping regime is still dominant in the power spectrum. It is also seen that the flapping regime is still modulated, but now the modulation includes the harmonics of the f_2 . The shape of the attractor has become more complicated: it is formed by three tori, embedded in one another. The dimension of this attractor seems to be fractal ($D = 3.2$), and the maximum Lyapunov exponent is positive and equal to 0.01. Hence, the flapping dynamics appears to be described by a strange weakly chaotic attractor. This flapping regime can be considered as chaotic, even though the quasiperiodicity remains observable (cf. Nayfeh and Balachandran [41]). The

Poincaré section forms a ringlike structure consisting of relatively empty core regions surrounded by denser regions; see Fig. 4(d). This ringlike structure of the Poincaré section suggests that the chaotic flapping regime has arisen from quasiperiodicity. A strong indication of such a transition is that lines connecting successive points of the Poincaré section do not cross the central empty region; they perambulate around its perimeter, indicating low-frequency modulations, as also evidenced through the power spectra. Similar scenarios were found to occur when analyzing the results of experiments with longer filaments.

B. Bistability

When the filament is long enough, a peculiar phenomenon near the critical value for the onset of flapping was observed: The filament flaps for a while, stops, then flaps again, and so on. For the same values of the control parameter (flow speed), the two states (i.e., the stretched-straight and flapping states) coexist; we have referred to this phenomenon as switching oscillations. This is clearly a form of bistability. Other researchers, including Zhang *et al.* [25] and Connell and Yue [19], have reported another type of bistability in which the system in stretched-straight equilibrium can become oscillatory if a given perturbation is applied. However, the system

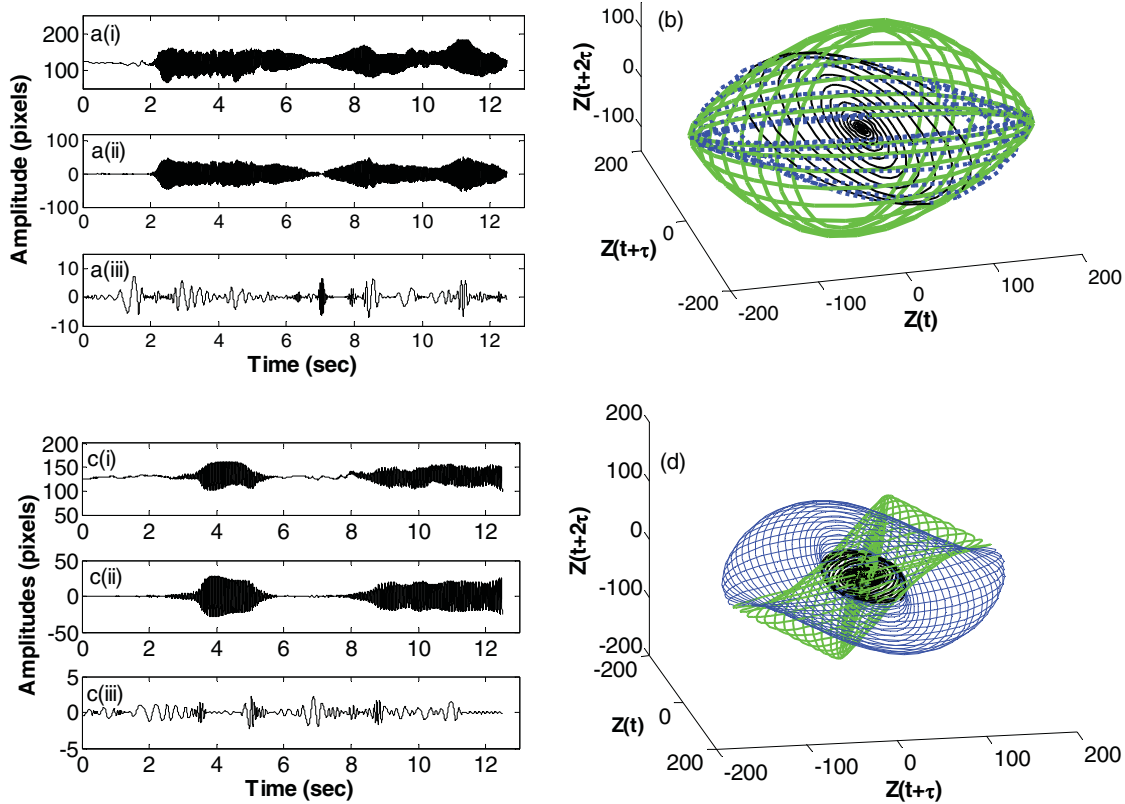


FIG. 5. (Color online) witching between stretched-straight and flapping solution: (a) time series of the cross-stream displacement of a point located at $\frac{3}{4}$ of a 6-cm-long filament for flow speed of 4.3 m/s: (i) raw time series, (ii) first intrinsic mode, and (iii) second intrinsic mode; (b) reconstructed attractor in principal basis from the time series of the cross-stream displacement in [a(ii)]; (c) time series of the cross-stream displacement of a point located at $\frac{3}{4}$ of a 10-cm-long filament for flow speed of 4.3 m/s: (i) raw time series, (ii) first intrinsic mode, and (iii) second intrinsic mode; and (d) reconstructed attractor in principal basis from the time series of the cross-stream displacement in [c(ii)].

never reverts to its original static state. The phenomenon called here switching oscillations differs from that in the foregoing studies in two significant ways: (i) it switches continuously from one state to the other, back and forth, and (ii) it does so *without any external perturbation*. The only perturbations to which the filament is exposed are those of the flow.

To illustrate this peculiar dynamics, the raw time series and its first two intrinsic modes for two filaments, 6 and 10 cm long, are shown in Figs. 5(a) and 5(c). In the first case, the time spent in the stretched-straight position is relatively short in comparison to the time intervals during which the filament was flapping. However, in the second case, the time spent in the stretched-straight position is longer. It is important to emphasize that the observed switching oscillation phenomenon is not circumstantial; it is repeatable and has also been observed in our laboratory with long flags placed in axial flow within a wind tunnel [42]. It is observed also that the filament relaxes into a stretched-straight state after transient damped oscillations; this suggests that the stationary regime (fixed point in phase space) is linearly stable with complex eigenvalues. A better description of this switching oscillation phenomenon is presented in phase space. In Figs. 5(b) and 5(d), one can clearly observe a bifurcation from a fixed point into a first limit cycle [black into blue (dark gray) lines] and afterward into a transverse limit cycle [green (light gray) lines].

The two transverse limit cycles form a 2D torus due to the modulation of the flapping by the low-frequency component, as detailed in the previous section. The fixed point represents a stationary solution, while the limit cycles represent the modulated oscillatory state or flapping state. We emphasize that the bistability behavior reported here, which consists of continuous switching between the two stationary states of the system, namely stretched-straight and periodic flapping, was observed in flow conditions where the flow velocity was low and the film thickness was small. The soap-film flow can be considered as fluctuation free (no striations or interferences were observed). It is less likely that such behavior is related to fluctuations in the flow. Because the flow velocity was near its critical value at which the filament should start flapping, the straight-stretched and flapping states should be close to each other. This bistability phenomenon can be seen as the complex oscillation (back and forth) between these two states.

Such switching oscillation phenomena have been observed in oscillating chemical reactions in a continuously stirred tank reactor (CSTR), where the system oscillates between stationary and oscillatory states. This particular phenomenon was associated with a subcritical Hopf bifurcation; see Boissonade [43]. It is worth noting that similar but less complex switching was observed in many systems but between

two unstable stationary solutions. In these systems, the solution goes from one unstable stationary solution to another, thereby performing a limit-cycle-like oscillation; see Refs. [44–46].

IV. CONCLUSION

In this study, the flapping dynamics of a filament placed in 2D soap-film flow is investigated. The results show that flapping is quasiperiodic, with the main flapping oscillation modulated by small-amplitude, small-frequency component. There may exist a narrow range of flow velocities where the

flapping was periodic prior to its becoming quasiperiodic, but this was not captured, perhaps because of the relatively high Reynolds number. The transition to the chaotic flapping state was shown to follow a quasiperiodic route. Moreover, this paper reports a robust new phenomenon named here “switching oscillation,” where the filament behavior continuously switches between the stretched-straight and flapping states. This switching oscillation is distinct from the bistability reported in previous studies, in that (i) no external perturbation is needed to initiate it and (ii) the system continuously alternates between the two states back and forth (not just once).

-
- [1] L. Rayleigh, *Proc. Lond. Math. Soc.* **10**, 4 (1879).
- [2] E. H. Dowell, *Aeroelasticity of Plates and Shells* (Noordhoff International Publishing, Leyden, 1975).
- [3] M. P. Paidoussis, *Fluid-Structure Interactions: Slender Structures and Axial Flow*, Vol. 2 (Elsevier Academic Press, London, 2004).
- [4] M. Shelley and J. Zhang, *Annu. Rev. Fluid Mech.* **43**, 449 (2011).
- [5] A. Kornecki, E. H. Dowell, and J. O’Brien, *J. Sound Vibrat.* **47**, 163 (1976).
- [6] L. Huang, *J. Fluids Struct.* **9**, 127 (1995).
- [7] T. Theodorsen, General Theory of Aerodynamic Instability and the Mechanism of Flutter. NACA Report 496, U.S. Nat. Advisory Committee for Aeronautics, Langley, VA (1935).
- [8] N. Yamaguchi, K. Yokota, and Y. Tsujimoto, *ASME: J. Fluids Eng.* **122**, 65 (2000).
- [9] Y. Watanabe, S. Suzuki, M. Sugihara, and Y. Sueoka, *J. Fluids Struct.* **16**, 543 (2002).
- [10] T. Balint and A. D. Lucey, *J. Fluids Struct.* **20**, 893 (2005).
- [11] C. Q. Guo and M. P. Paidoussis, *J. Appl. Mech.* **67**, 171 (2000).
- [12] C. Eloy, C. S. R. Lagrange, and L. Schouveiler, *J. Fluid Mech.* **611**, 97 (2008).
- [13] C. Eloy, C. Souilliez, and L. Schouveiler, *J. Fluids Struct.* **23**, 904 (2007).
- [14] M. Argentina and L. Mahadevan, *Proc. Natl. Acad. Sci. USA* **102**, 1829 (2005).
- [15] L. Tang and M. Paidoussis, *J. Sound Vibrat.* **305**, 97 (2007).
- [16] S. Alben and M. J. Shelley, *Phys. Rev. Lett.* **100**, 074301 (2008).
- [17] S. Michelin, S. Llewellyn-Smith, and B. Glover, *J. Fluid Mech.* **617**, 1 (2008).
- [18] L. D. Zhu and C. Peskin, *J. Comput. Phys.* **179**, 452 (2002).
- [19] B. Connell and D. Yue, *J. Fluid Mech.* **581**, 33 (2007).
- [20] S. Taneda, *J. Phys. Soc. Jpn.* **24**, 392 (1968).
- [21] N. Yamaguchi, T. Sekiguchi, K. Yokota, and Y. Tsujimoto, *ASME: J. Fluids Eng.* **122**, 74 (2000).
- [22] Y. Watanabe, S. Suzuki, M. Sugihara, and Y. Sueoka, *J. Fluids Struct.* **16**, 529 (2002).
- [23] D. M. Tang, H. Yamamoto, and E. H. Dowell, *J. Fluids Struct.* **17**, 225 (2003).
- [24] M. Shelley, N. Vandenbergh, and J. Zhang, *Phys. Rev. Lett.* **94**, 094302 (2005).
- [25] J. Zhang, S. Childress, A. Libchaber, and M. Shelley, *Nature (London)* **408**, 835 (2000).
- [26] D. Georgiev and P. Vorobieff, *Rev. Sci. Instrum* **73**, 1177 (2002).
- [27] M. A. Rutgers, X. L. Wu, R. Bhavagatula, A. A. Petersen, and W. I. Goldburg, *Phys. Fluids* **8**, 2847 (1996).
- [28] D. A. Dadeppo and R. Schmidt, *Textile Res. J.* **41**, 911 (1971).
- [29] Y. Couder, J. M. Chomaz, and M. Rabaud, *Phys. D (Amsterdam, Neth.)* **37**, 384 (1989).
- [30] M. Gharib and P. Derango, *Phys. D (Amsterdam, Neth.)* **37**, 406 (1989).
- [31] B. Martin and X. Wu, *Rev. Sci. Instrum.* **66**, 5603 (1995).
- [32] X. Wu, R. Levine, M. Rutgers, H. Kellay, and W. Goldburg, *Rev. Sci. Instrum.* **72**, 2467 (2001).
- [33] A. Roshko, On the Development of Turbulent Wakes from Vortex Streets. NACA TN-2913, National Advisory Committee for Aeronautics, Washington, DC (1953).
- [34] O. Greffier, Y. Amarouchene, and H. Kellay, *Phys. Rev. Lett.* **88**, 194101 (2002).
- [35] N. H. Packard, J. P. Crutchfield, J. D. Farmer, and R. S. Shaw, *Phys. Rev. Lett.* **45**, 712 (1980).
- [36] F. Takens and R. Mañé, in *Dynamical Systems and Turbulence*, Lecture Notes in Mathematics, edited by R. Rand and L. S. Young (Springer, Berlin, 1981).
- [37] P. Grassberger and I. Procaccia, *Phys. D (Amsterdam, Neth.)* **9**, 189 (1983).
- [38] A. M. Albano, J. Muench, C. Schwartz, A. I. Mees, and P. E. Rapp, *Phys. Rev. A* **38**, 3017 (1988).
- [39] N. E. Huang, Z. Shen, S. R. Long, M. C. Wu, H. H. Shih, Q. Zheng, N. C. Yen, C. C. Tung, and H. H. Liu, *Proc. R. Soc. London A* **454**, 903 (1998).
- [40] P. Bergé, Y. Pomeau, and C. Vidal, *Order within Chaos* (Hermann, Paris, 1984).
- [41] A. H. Nayfeh and B. Balachandran, *Applied Nonlinear Dynamics* (John Wiley & Sons, New York, 1995).
- [42] H. A. Abderrahmane, M. P. Paidoussis, M. Fayed, and H. D. Ng (unpublished).
- [43] J. Boissonade, *J. Chim. Phys.* **73**, 540 (1976).
- [44] K. L. C. Hunt, P. M. Hunt, and J. Ross, *Annu. Rev. Phys. Chem.* **41**, 409 (1990).
- [45] J. Boissonade and P. D. Kepper, *J. Phys. Chem.* **84**, 501 (1980).
- [46] M. Berhanu *et al.*, *J. Fluid Mech.* **641**, 217 (2009).